AD NUMBER

AD820349

NEW LIMITATION CHANGE

TO

Approved for public release, distribution
unlimited

FROM

Distribution authorized to U.S. Gov't.
agencies and their contractors; Critical
Technology; AUG 1967. Other requests shall
be referred to Air Force Rocket Propulsion
Lab., Attn: RPPR-STINFO, Edwards AFB, CA
93523.

AUTHORITY

AFRPL ltr dtd 27 Oct 1971

FEASIBILITY DEMONSTRATION OF A ROCKET ENGINE ABLATION GAUGE TASK II SUMMARY REPORT

Technical Report AFRPL-TR-67-218
August 1967

**BEST
AVAILABLE COPY**

FEASIBILITY DEMONSTRATION OF A
ROCKET ENGINE ABLATION GAUGE
TASK II SUMMARY REPORT

Technical Report AFRPL-TR-67-218
August 1967

Prepared for
AIR FORCE ROCKET PROPULSION LABORATORY
Edwards Air Force Base California 93523

Contract AF 04(611)-11413

FOREWORD

This report was prepared by TRW Systems for the Air Force Rocket
Propulsion Laboratory, Air Force Systems Command, under Contract
AF 04(611)-11413. Project monitor for the Air Force Rocket
Propulsion Laboratory was Mr. Wallace Buchholtz (RPFTR). The
work covered by this report was conducted from September 1966
through April 1967.

Acknowledgement is given to Messrs. R. J. Rusch, J. F. Jones,
R. T. Fabian, W. H. Chollman, W. B. Turner, and Mrs. S. Venne
for their contributions to this report.

This report has been reviewed and is approved.

Wallace L. Buchholtz
AFRPL (RPFTR), Project Engineer

ABSTRACT

This report describes the work performed by TRW Systems during the
second phase of the 12-month program entitled, "Feasibility Demonstration
of a Rocket Engine Ablation Gauge." This program has been supported
and directed by the Air Force Rocket Propulsion Laboratory under
Contract AF 04(611)-11413. The objective of the program is to demon-
strate the feasibility of dynamically measuring ablation and erosion
rates of rocket nozzle liners. The measurement technique employs trace
quantities of two radioactive compounds which are embedded in the noz-
zle at selected locations. The compounds are chosen so that one ablates
and the other erodes in the same manner as the surrounding nozzle mater-
ial. Ablation and erosion depths are determined from the decrease in
radiation intensity measured external to the nozzle shell. The Air
Force selected a carbon phenolic, MX4926, as the nozzle material of
interest for this program. Studies include analyses to establish
design parameters (Task I), laboratory experiments to evaluate test
variables (Task II), and five tests of a 5000-pound thrust, liquid
propellant rocket engine to demonstrate the measurement technique
(Task III). This report covers Task II, during which laboratory equip-
ment was designed and built to fabricate recession sensor needles,
measure incremental radiotracer uniformity along needle lengths, and
perform needle/material recession tests in an oxyacetylene flame.
Carbon phenolic needles, containing both inert and radioactive additives
were fabricated to a nominal density of 1.35 gm/cm^3, which is 94 percent
of the acceptable density of the virgin MX4926 material. The ablation
measurements employed a ^{113}Sn-$^{113}InCl_2$ tracer; $^{46}Sc_2O_3$ was used as the
erosive tracer. Variations in the radiotracer distribution were
measured in 100-mil increments along the length of the fabricated
needles and were typically within 3 percent of the mean. The effects
of source-detector geometry, system configuration, and overall system
response were evaluated experimentally. In oxyacetylene flame-tests,
both ablative and erosive gauging measurements were within 20 mils of
the physically-measured values.

Table of Contents

Figures

1.0 INTRODUCTION

Ablative rocket-nozzle technology has lacked an accurate method for dynamically measuring ablation and erosion rates during rocket engine test firings. The objective of this program is to demonstrate the feasibility of a measurement technique which employs trace quantities of two radioactive compounds which are locally embedded in the nozzle. The compounds are selected so that one ablates and the other erodes in the same manner as the surrounding nozzle material. Ablation and erosion depths are determined from the decrease in radiation intensity measured external to the engine shell. The Air Force selected a carbon phenolic, MX4926, as the nozzle material of interest for this program.

The program is divided into three tasks: system analyses and design, a laboratory test program, and a 5K engine test program. During the first task, appropriate radiochemical materials were selected and analyses performed to relate radiation intensity changes outside the engine to the ablation and erosion depths of the nozzle material. Gauging hardware for 5K engine tests was also designed during the first task. These efforts are discussed in, "Feasibility Demonstration of a Rocket Engine Ablation Gauge, Task I Summary Report", (AFRPL-TR-66-313).

The studies conducted during the second task of the project are the subject of this report. Task II, entitled, "Laboratory Test Program", included sensor needle fabrication studies and laboratory-scale testing.

The use and meaning of the terms "ablation" and "erosion" vary widely. Within this report, the term "ablation" is synonymous with "charring". The "char" depth includes both the pyrolized material and the decomposition zone. Figure 1 shows an ablative nozzle section as viewed after an engine test. The different areas are marked in the magnified view of the nozzle-section; the darkest area is the decomposition zone separating the virgin and char layers. "Erosion" as used in this report, connotes the physical removal of the charred material, and is synonymous with "char recession". The term "needle" is used to describe the slender cylinders of nozzle material which contain the ablation and erosion radiocompounds.
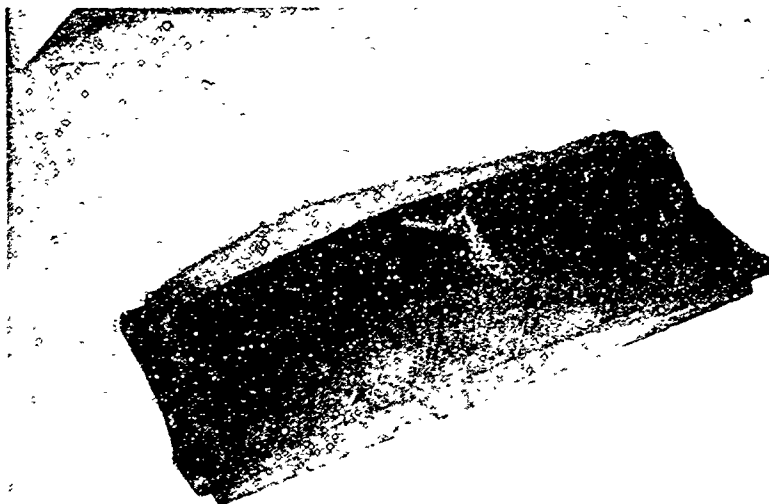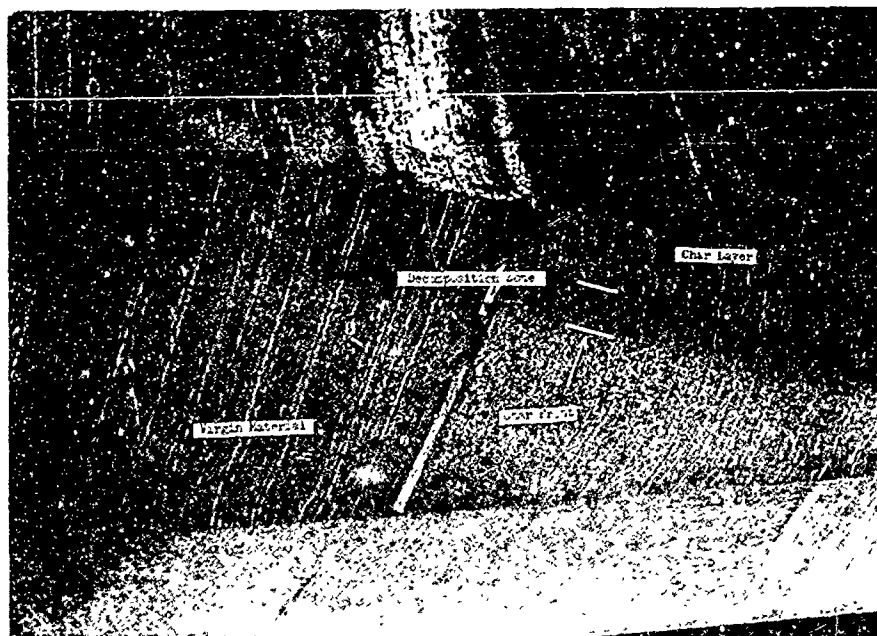
Figure 1. Cross Section of Tested Ablative Nozzle

Closeup of Nozzle Cross Section

1-2

2.0 NEEDLE FABRICATION STUDIES

To assess the ablation and erosion of the rocket nozzle dynamically during a test firing, the needles must behave in the same manner as the ablative material. If the needles can be fabricated with a material composition and density which closely approximates the nozzle material, their response to the engine environment will closely resemble that of the ablative material. Since gauging measurements are obtained by observing the loss of radioactive material from the needles, non-uniformity in radiotracer concentration along the length of the needle will cause gauging measurement inaccuracies. For maximum precision in gauging measurements, one must either account for the effects of density and activity variations or reduce the magnitude of these variables to a tolerable level. For simplicity of gauge operation, the latter approach is by far the more preferable.

Among the needle fabrication techniques considered were the addition of inert tracers to the ablative matrix with subsequent radio-activation by neutron bombardment[1], impregnation of the ablative material with solutions or slurries which are subsequently evaporated[2,3], and addition of radiotracer to a matrix other than the ablative material[4,5]. The technique selected for application in this program was a molding process with the addition of radioactive compounds to ablative material constituents just prior to needle fabrication. This technique permits thorough material mixing to achieve radiotracer distribution uniformity while still providing a fabricated product which very closely resembles the virgin nozzle material.

The present program involves only one ablative nozzle material; hence development of the fabrication process was specific. However, the basic technique offers flexibility for application to recession gauging studies of other ablative materials.

The molding apparatus which was used in the Task II studies is illustrated in Figure 2. With this mold, one to six needles can be fabricated at the same time. The individual needles are formed in 0.125 inch I.D. by 2.5 inch long drill bushings of case-hardened steel. Pressure is applied to the needles in the molds through 0.122 inch diameter by 0.375 inch long pins of mild steel. Caps screws extending
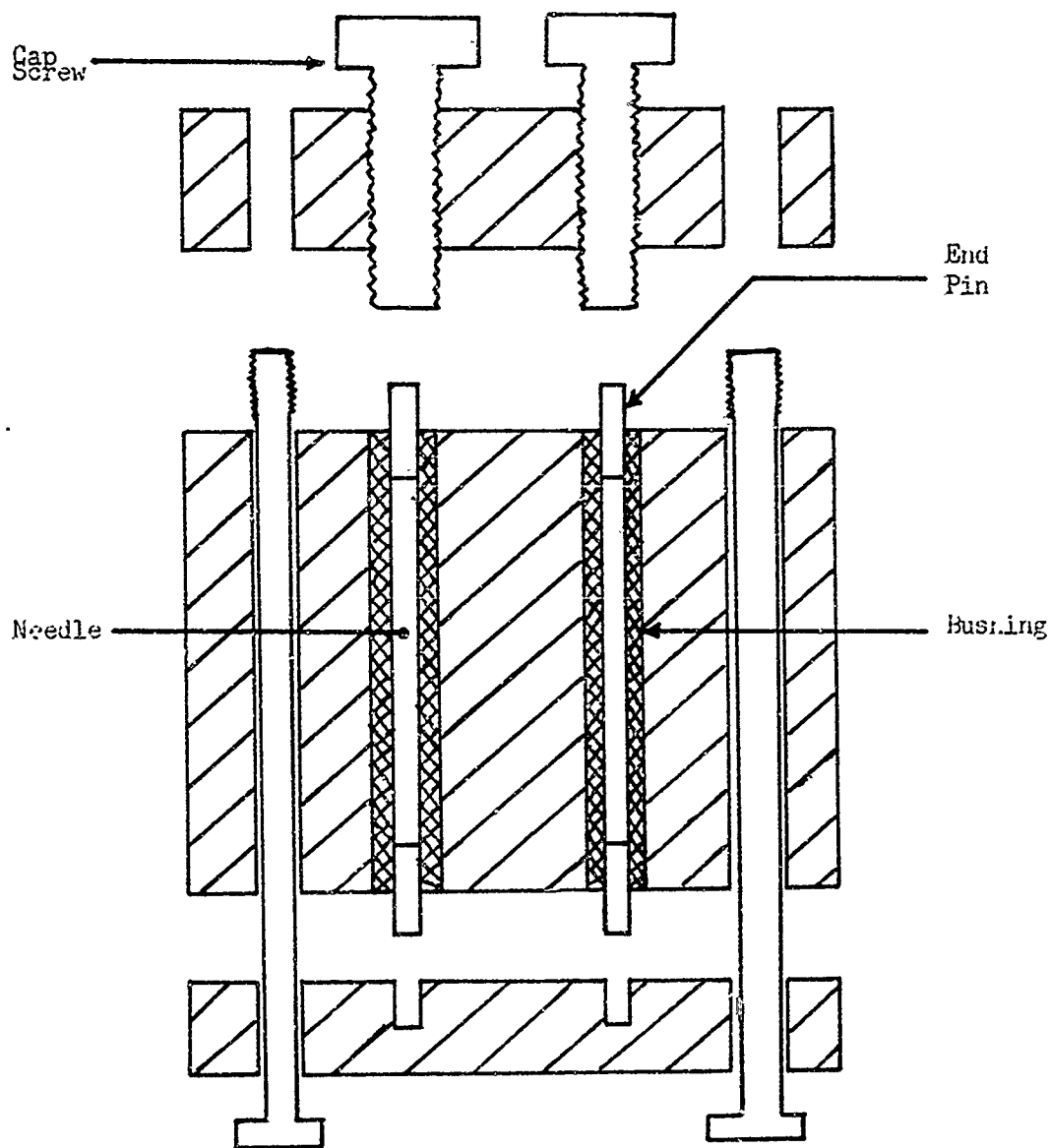
Figure 2. Needle Molding Apparatus

through one end plate allow compensation for differences in loading density of individual needles. During the molding process, a portion of each end pin extends from the bushing for ease of removal. Before initiation of the thermal curing process, pressure is applied to the upper end plate with a hydraulic press. This pressure is maintained during thermal cure with the six bolts about the perimeter of the mold.

2.1 Inert Needles

Initial studies were conducted with inert tracer chemicals. These studies provided experience in the operational procedures of the fabrication process. During this effort, the physical characteristics of inert needles within a single batch and of different batches were evaluated. Table I illustrates the needle density variations within different fabrication batches.

The ablation and erosion rates are greatly affected by the density of material, regardless of the propellant environment[6]. In the absence of definitive data on which to base needle density rejection/acceptance criteria, a minimum value of 1.12 gm/cm^3 (80 percent of acceptable MX4926 density) was selected. A value of 1.26 gm/cm^3 (90 percent of acceptable MX4926 density) was adopted as the design goal.

Because of the importance of density, the techniques used to determine this parameter merits discussion. When used in this report, "density" connotes gross needle density. To determine this density, the mass is obtained gravimetrically and volume is determined by micrometer measurement. The principal error in the density determination is the measurement of needle diameter. With a nominal diameter of 124 mils, this dimension can vary along the length of any needle by as much as 2 mils. Four separate measurements of the diameter are taken along the needle diameter. It is estimated that the mean diameter value is accurate to within 1 mil. However, an error of this magnitude will produce a 1.6 percent error in the volume and hence in the resultant density value.

To confirm the diametral measurement accuracy, a needle volume was experimentally determined by both dimensional measurements and

Table I. Needle Batch Density Variations

	Batch				
	A	B	C	D	E
Individual Needle Densities (gm/cm^3)	1.374	1.396	1.423	1.391	1.372
	1.329	1.372	1.414	1.345	1.319
	1.281	1.346	1.351	1.334	1.281
	1.200	1.320	1.314		1.234
		1.237	1.294		
Group Average Density (gm/cm^3)	1.29	1.33	1.36	1.36	1.30

Overall average density 1.330 ± 0.058 gm/cm^3 at 1σ

water mass displacement. In the latter method, irregularities in the diameter are inherently accounted for. The density from the dimensional method was 2.1 percent less than that of the displacement method. However, data presented in Section 4.3.1 (Erosion Flame Tests) show uncertainities of this magnitude do not impair the performance of the gauge.

Different mixture ratios of carbon fiber/phenolic binder, and various molding pressures, cure times, and temperatures were tried during the inert needle fabrication studies. With a low weight percentage of phenolic binder, the mixture was difficult to pack into the molds and needle integrity could not be maintained. With high phenolic binder concentrations, nominal needle densities of 1.26 gm/cm^3 could not be obtained without excessive molding pressures and substantial resin leakage from the mold. Long cure times and high cure temperatures made needles difficult to remove from the mold; the resultant needles were of lower density and had surface irregularities. When either time or temperature was significantly reduced, the needles did not cure; they were flexible and continued to lose weight for a period of days after fabrication. Other forms of the carbon cloth and powdered carbon additives were tried as mold materials, but the resulting needles did not exhibit satisfactory physical integrity or density.

The most satisfactory needle molding mixture was found to be 67 weight percent of MX4926* material and 33° weight percent of phenolic binder. The MX4926 material was mascerated into fiber lengths of 60-100 mils. The phenolic binder used in the needle molding was the same resin used by the manufacturer during his impregnation process, except that it lacked the carbon filler. The needle ingredients were packed into the molds and 2200 psi of pressure was applied until the molding jig maintained that pressure. The mixture was then cured for 2 hours at 300-350°F. The needles were removed while the mold was still hot.

---

*The MX4926 fabric is carbon cloth (HITCO CCA-1) which has been impregnated with a high-temperature phenolic resin content of 32-37 percent. Reinforcement is obtained by addition of a fine resin filler of carbon during the CCA-1 cloth impregnation.

The selected needle molding mixture and technique yielded needles of uniform and acceptable density. Resin leakage with a resultant loss of tracer additives during molding was minimal. Physical integrity of the needles was satisfactory and the virgin MX4926 was closely simulated. The tracer additives were firmly held within the resin binder which minimized their loss through surface abrasion and handling.

After establishing the critical parameters of the molding fabrication technique (time, temperature, pressure, and mixture ratio), needles were made with radiotracer additives.

2.2 Radioactive Needles

The radioactive needles fabricated during the Task II effort contained a nominal 10-microcurie quantity of one or more selected radiochemicals. This is approximately 1 percent of the licensed radioactive amounts for 5K engine tests. The smaller quantities were used to minimize both personnel radiation exposures and activity release during laboratory flame tests.

When received from the supplier, the radiotracers were in solution. The tracers were converted to the selected chemical form prior to mixing with the phenolic binder. The binder material was then added to the carbon fibers and the fabrication procedure thereafter was identical to that described in the previous section.

During each step of the fabrication sequence, radiation intensity measurements were made to maintain process control and radiotracer accountability. An initial measurement was made in a fixed source-detector geometry and with a known amount of radioactivity. After each succeeding process operation, additional measurements were taken in the same geometry for comparison to the initial intensity value. Since activity losses to 50 percent or more occur during the complete sequence of needle fabrication, careful process control is required to obtain the desired amount of radiotracer per unit length in the finished needles.

Uniformity of tracer concentration along the length of the radioactive needles was determined by measuring their radiation intensity through a slit collimator of lead. The gamma radiation was detected with a 2 by 1.5 inch diameter sodium-iodide scintillator during a major portion of the uniformity studies. A thin plastic scintillator was used in later measurements of incremental gamma intensity. Neither detection configuration was completely satisfactory because increments adjacent to the one being measured also contributed to the detected radiation intensity. This contribution, the manner in which it was determined, and the resultant corrective measures taken are discussed in Appendix I (Incremental Uniformity Analyses).

3.0 LABORATORY SCALE TESTING

Experimental studies were performed with inert and radioactive needles to observe the effects caused by adhesives, adjacent ablative materials, and exposure to heat and flame.

3.1 Inert Needle Tests

Successful application of the ablation gauging technique requires that the needles react to a heat flux in the same manner as the surrounding nozzle material. Laboratory flame-tests were first performed with inert needles to determine an appropriate means of retaining the needles in the MX4926 ablative material without heat flux perterbations. Through testing with the oxyacetylene torch, assessment was made of adhesive material influence upon heat conduction. Three adhesive materials were studied; two epoxies and a ceramic material. The physical reaction of the needles to heat flux was observed concurrent with the adhesive evaluations.

Inert needles were mounted in MX4926 blocks and exposed to the oxyacetylene flame. Figure 3 shows a needle partially inserted into the sample block. As Figure 4 illustrates in cross-section view, the flame test apparatus included mounting fixtures for the test sample, the torch, and a radiation detection assembly. A thermal barrier was placed between the sample and the detector to prevent detector damage. Figure 5 shows the assembled flame-test hardware.

The flame testing apparatus provided a thermal environment to cause both ablation and erosion of the test sample. Because the apparatus could not reasonably approximate the engine test environment, no direct thermal flux measurements were made of the flame testing apparatus. However, from knowledge of oxygen/acetylene pressures and flow rates, an approximate heat flux value of 1060 BTU/ft^{2}sec was determined. Using data reported by Davis[5] relating ablation, time, and heating rate of a similar heat shield material, and with knowledge of our ablation rates, a heat flux value of 1130 BTU/ft^{2}sec was determined for our apparatus. From the close agreement between two independent calculation procedures it can be concluded that the nominal heat flux was close to 1100 BTU/ft^{2}sec.
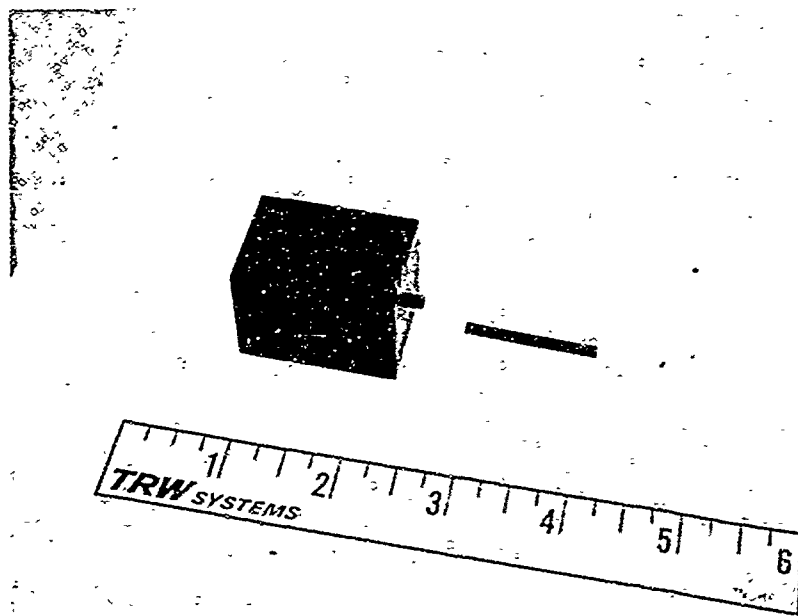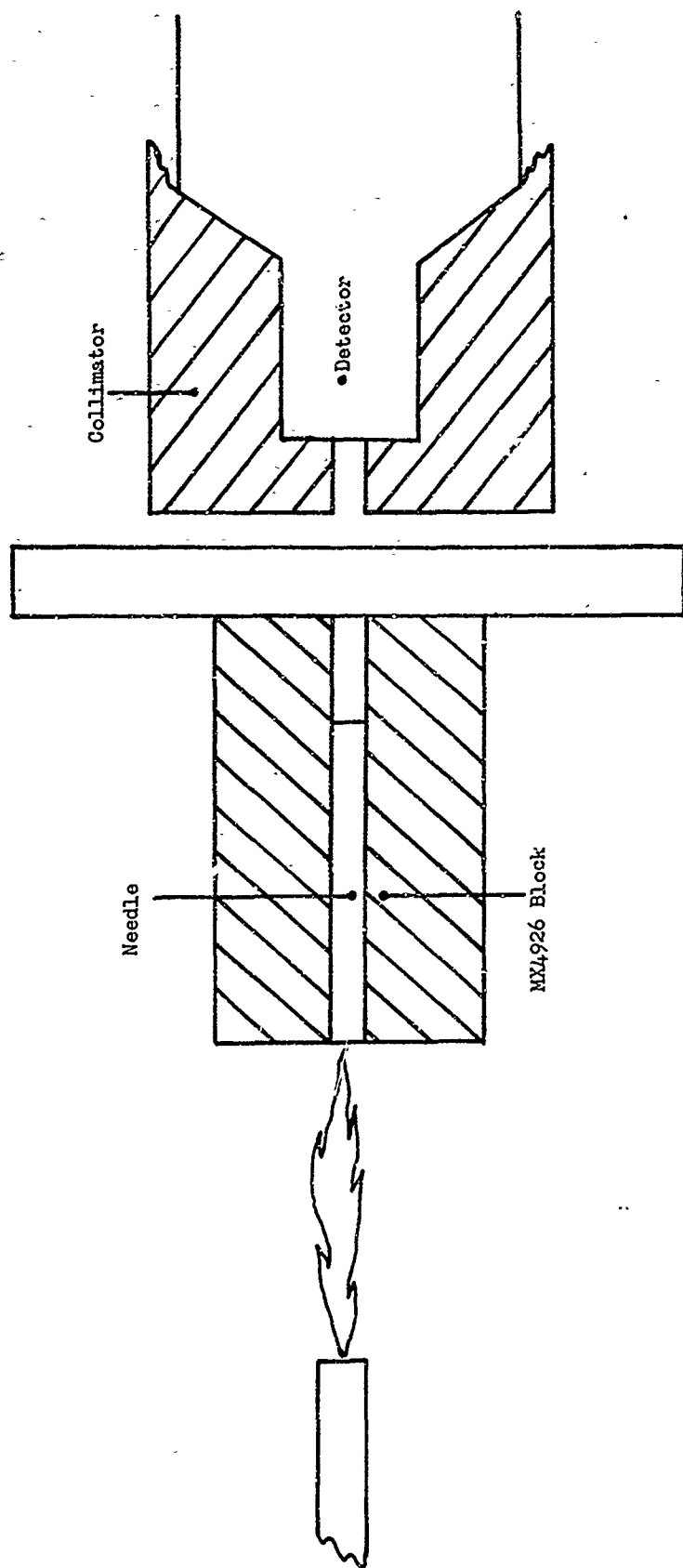
Figure 3.   Needles and MX4926 Sample

Figure 4. Cross Section of Flame-Test Apparatus

Collimator

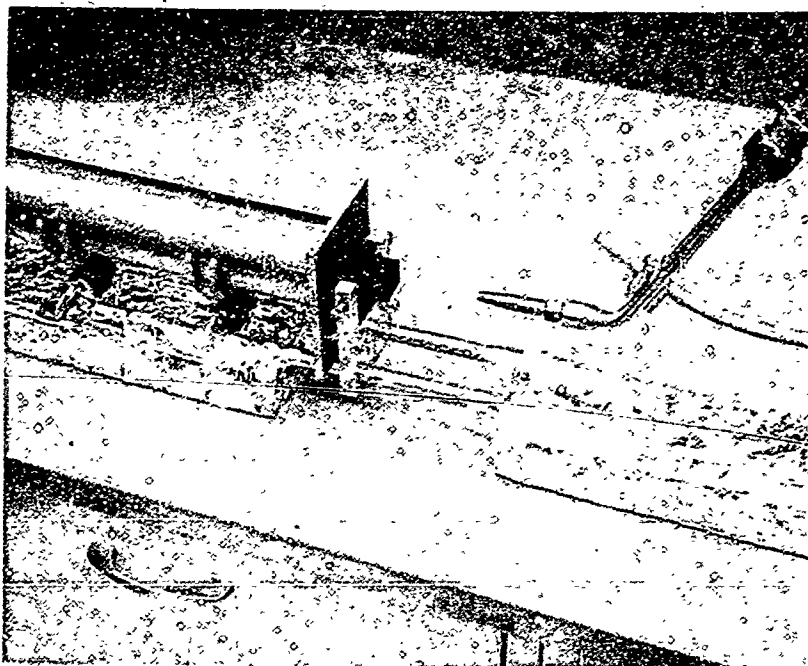•Detector

Needle

MX4926 Block

3-3

Figure 5. Flame-Test Assembly

During the flame tests, both the physical integrity of the needle and the thermal topography of the needle and test block were observed through a micro-optical pyrometer. The pyrometer has an object resolution of 10 mils at a distance of three feet from the sample and a temperature discrimination capability of $10°F$ at temperatures up to $1900°F$.

The MX4926 ablative material is a laminate of carbon cloth and thus the carbon strands are specifically oriented. On the other hand, the needles were made from short pieces of carbon cloth strands which take a random orientation in the needle. It was suspected that this difference in fiber orientation might result in different ablation and erosion rates. No such difference was observed in the laboratory testing.

From the inert needle flame tests, it was determined that any of the three adhesive materials could be successfully used to hold needles in place. Testing also showed that a diametral clearance of approximately 4 mils between the needle and its hole allowed a minimum use of adhesives and provided best results. Larger clearances, and hence additional adhesive volumes, resulted in needle erosions as much as 20 mils less than that of the virgin material. Pyrometer readings indicated that the needle temperature was 40 to $100°F$ lower than the surrounding material at temperatures in the 1500 to $1700°$ range. Under the same test conditions, but restrictive adhesive use and a close needle/hole fit, no temperature difference could be observed between the needle and virgin sample block. Each of the three adhesives will be used in the first 5K engine nozzle to confirm their individual performance under actual test conditions.

Figure 6 shows some adhesive flame-test samples; an untested block is included for comparison. In the block on the left, the needle was held by epoxy adhesive. The block on the right employed a carbon-epoxy mixture, and in the third block from the left, no adhesive was used. Figure 7 is another view of this block with the needle partially removed. In this view, the char and decomposition zone are clearly defined. In post-test destructive examinations, it
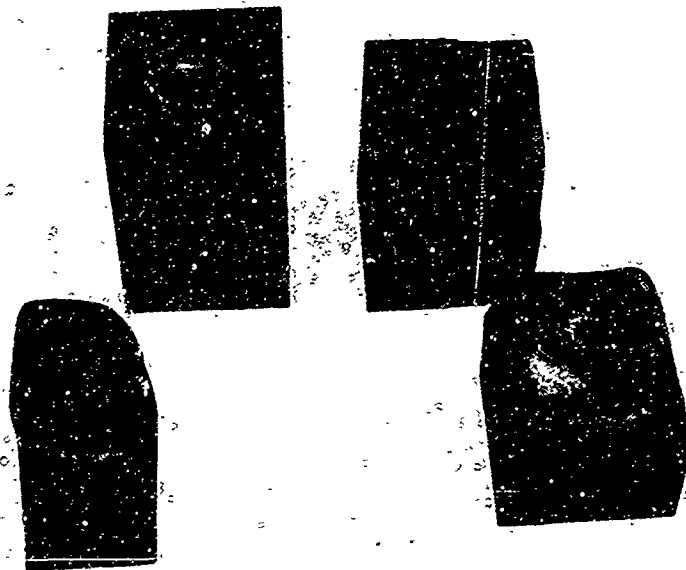
3-5

Figure 6. Ablative Samples

Figure 7.   Flame-Tested Needle and Block

was found that the ablation depth on the needles agreed with that of the adjacent MX4926 material.

3.2 Gauging Calibration Theory

A schematic diagram of the ablation gauging system is shown in Figure 7. For a single source with the geometry of Figure 8, the count rate at the detector is given by the relationship:

$$R = \frac{I \cdot S_1 A}{4\pi} \int_0^y \frac{\exp[-\mu x] \, dx}{(d + x)^2} \qquad (1)$$

where:

R = count rate (counts/sec)

$I \cdot$ = detector sensitivity $\left(\frac{\text{counts/sec}}{\text{photons/cm}^2\text{-sec}}\right)$

S_1 = source strength per unit length (photons/cm-sec)

d = distance from end of source needle to detector (cm)

μ = linear absorption coefficient of ablative material (cm^{-1})

y = length of source remaining (cm)

A = absorption in materials other than the source needle (engine casing, adhesive, etc.)

The term which precedes the integral in equation (1) remains constant for any given test configuration. Only the values of y and μ change during the test and the latter change is so slight it can be ignored as discussed below.

The linear absorption coefficient of the ablative material, μ, is dependent upon three factors: gamma energy, absorber composition, and absorber density. Both absorber composition and density change during a test. The ablative source gammas pass through the virgin material before being detected, but the eroder gammas traverse both virgin and char materials. Only in the eroder source evaluation does μ change as pyrolysis occurs. Through selection of an eroder source with energetic gammas, the effect on μ can be made insignificant. This was experimentally demonstrated in the erosion flame test studies.
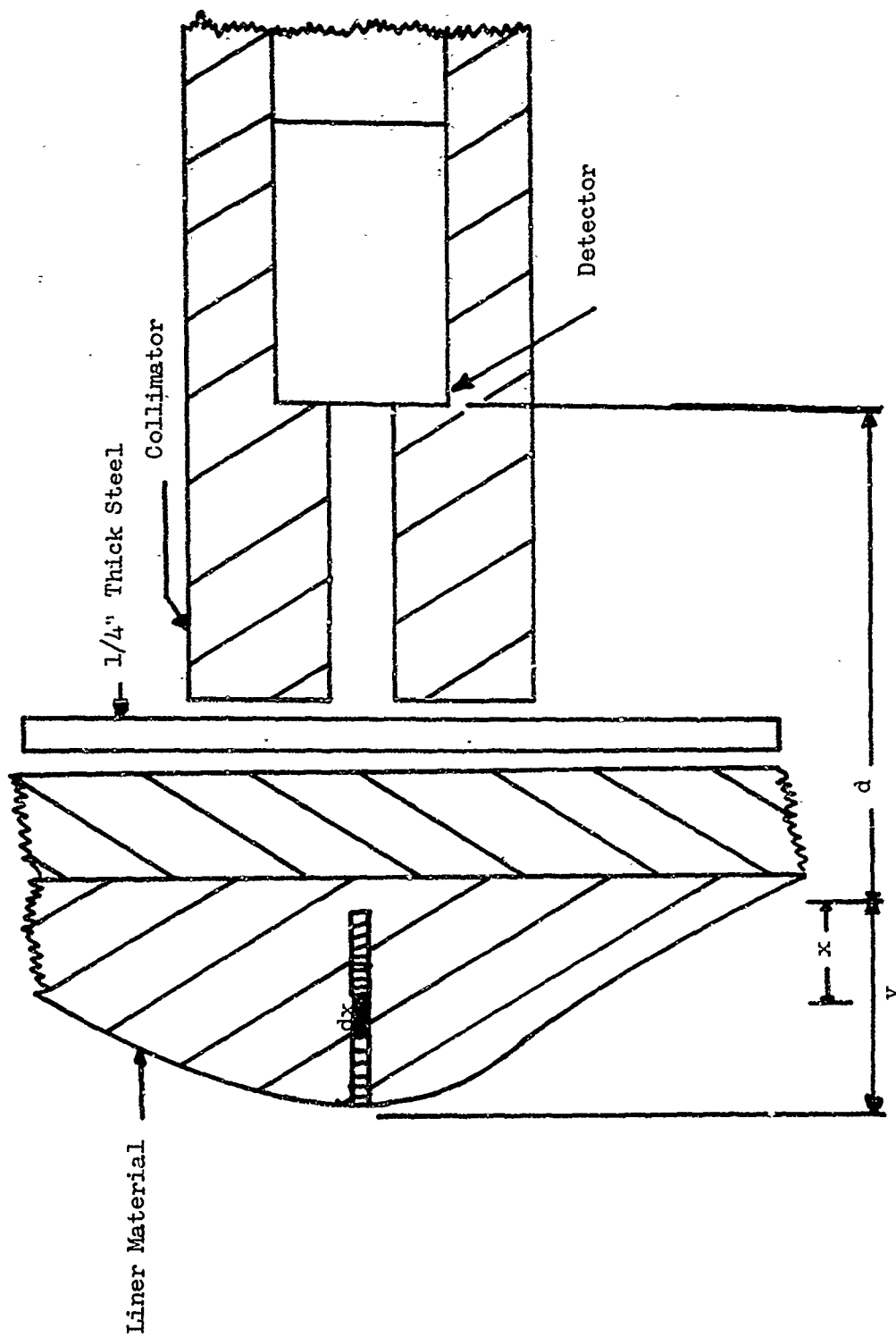
Figure 8. Schematic of Ablation Gauging System

By evaluating the integral $I(y) = \int_0^y \frac{\exp[-\mu x]\,dx}{(d + x)^2}$ for specific needle lengths of a given source and geometry, one can determine the relationship between the change in count rate and change in needle length. This relationship is used to obtain the theoretical calibration curves; an example of which is shown in Figure 9. The curvature above a negative 45-degree slope results from the decrease in average attenuation thickness and the changing source-detector geometry.

3.3 Recession Flame Tests

Measurements of ablation and erosion with the radiotracer technique were obtained under controlled laboratory conditions. The tests were conducted in an open-faced hood using the flame-testing apparatus previously described. Airborne radioactive material released during the tests was retained in the hood exhaust filter.

In the flame tests, physical measurements of total erosion were taken with a micrometer depth gauge extended from a fixed reference point external to the char surface of the test block in the area of the needle. These measurements were accurate to within 0.5 mil.

Prior to ablation testing in the laboratory, it had been planned that ablative radiotracer gauging measurements would be compared to char-front measurements obtained with x-ray radiographs. This technique did not provide adequate precision for accurate calibration. The relatively small change in material density during the ablation process and radiograph "smearing" from char-front irregularities yielded physical measurement uncertainities in excess of 30 mils. These char-front irregularities, as exemplified in Figure 7, were probably accentuated by the use of an oxyacetylene torch and the small MX4926 samples.

To obtain satisfactory precision in char-front measurements it was necessary to relate tracer count rate (i.e., needle ablation) to the ablation of the immediately adjacent areas of the MX4926 sample. To accomplish this the sample block was cut near and parallel to the needle and then the pieces were clamped together for flame testing. In this was the total char-front recession could be observed

by interrupting the flame exposure and separating the sample sections. Recession data were obtained by measuring the virgin material thickness adjacent to the needle with a micrometer referenced to the test sample base.

3.3.1 Erosion Flame Tests

Measurements with the erosion radiochemical were performed first because better precision could be obtained with the physical measurements of that process. Thus, precise comparisons could be made between theory and experiment to establish and confirm the gauging calibration.

Erosion flame tests of radioactive needles were performed with the $^{46}Sc_2O_3$ erosion tracer. This isotope was selected as the first choice in preference to ^{95}Zr because of its higher gamma energy, greater abundance, and lower cost.

Figure 9 illustrates the theoretically-derived curve for the laboratory testing geometry along with the experimental data points for erosion tests of two needles having dissimilar densities. One needle density (Needle A) was 2.5 percent lower than the value used for the theoretical curve, the other (Needle B) was 5.9 percent above that value. The standard deviation of the erosion gauge errors was 5.1 mils, where the error is defined as the difference between the physically measured erosion and that determined by radiotracer measurement. With a one-inch needle length, this deviation is equivalent to a 0.5 percent error. As shown in Figure 9, excellent agreement exists even with erosion of less than 100 mils. From these tests, it was concluded that the ^{46}Sc tracer and the theoretical relationship between count rate and source needle length would be used to gauge erosion in the 5K engine tests. The agreement between theory and measurement demonstrated that empirical calibrations for the erosion gauging measurements would not be necessary.

3.3.2 Ablation Flame Tests

The task of relating a radiotracer vaporization loss to the MX4926 ablative process was more complex than the erosion studies
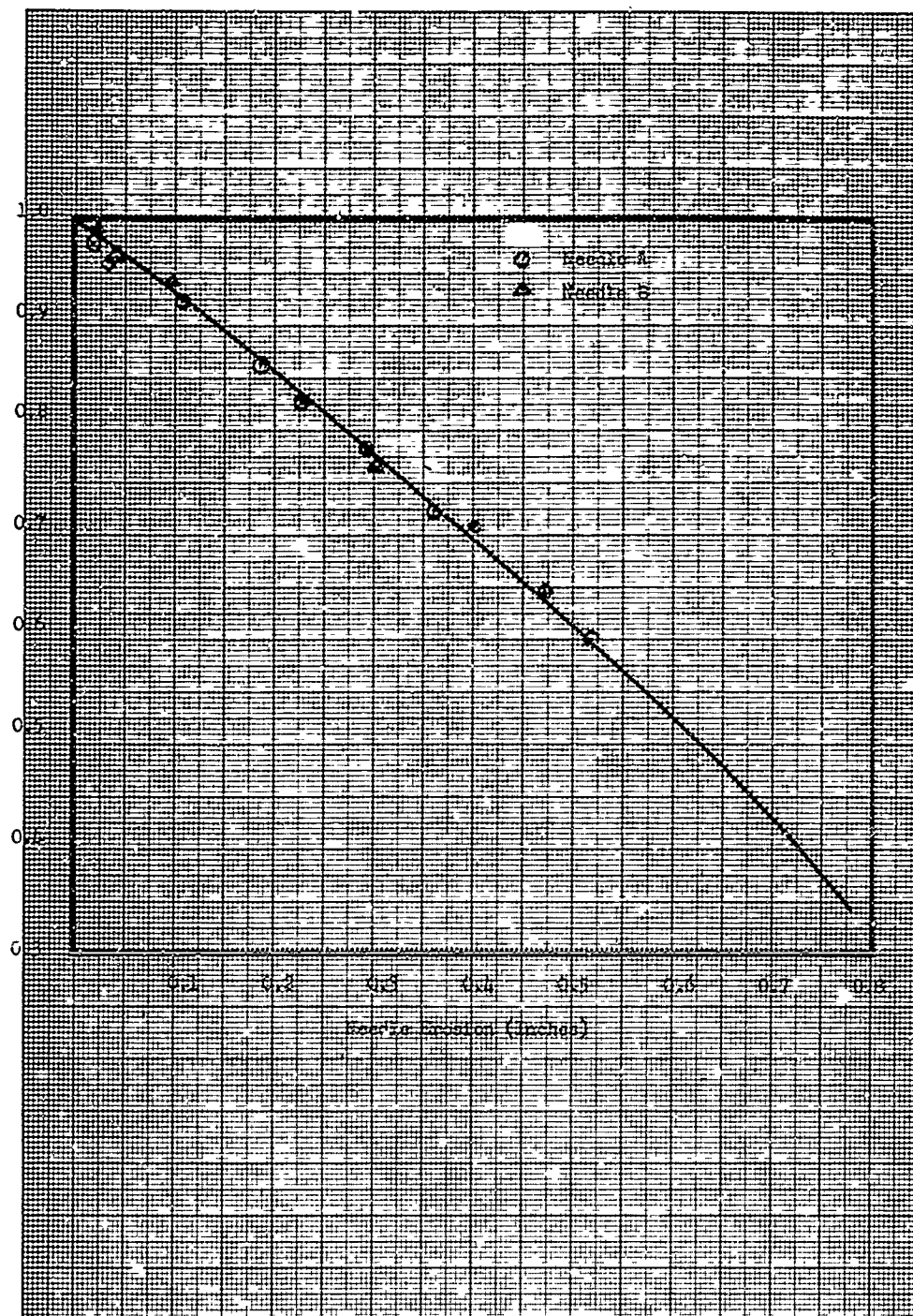
Figure 9. Erosion Gauging Measurements with $^{46}Sc_2O_3$

because radiotracer vaporization occurs at a discrete temperature while material ablation occurs over a broad range in temperatures. However, radiotracer vaporization and matrix material ablation have been successfully correlated for reentry heat-shield ablative materials[2,3,5].

Decomposition of phenolic ablative material occurs throughout the range of 350 to 850°C with the greatest material density change occuring between 550 and 600°C[7]. From thermogravimetric analyses (TGA) of the MX4926; one cannot attach a specific temperature corresponding to the pyrolysis-virgin material interface (char-front). A typical TGA* is illustrated in Figure 10.

Flame tests were performed with compounds of ^{203}Hg and ^{113}Sn to evaluate their effectiveness in ablation gauging measurements. Because of the significantly lower cost and the lower biological hazard of ^{203}Hg compared to ^{113}Sn, ablation flame testing was initiated with the radioactive mercury compounds.

3.3.2.1 Mercury Ablative Compounds

Prior use of ^{203}Hg compounds in heat-shield ablation studies yielded inconclusive results. Lang[3] reported both $HgCl_2$ and HgS volatilized at a reduced temperature when in a phenolic ablative matrix. Davis[5] reported successful application of HgS mixed with a plastic binder and contained in teflon tubes.

Because of possible discrepancies between the tracer vaporization and the temperature corresponding to the char-front, thermocouples were placed in the MX4926 sample block. The temperature sensors were located adjacent and normal to the needle axis (and hence to the flow of heat through the block). During the test, thermocouple temperatures were recorded as the count rate from the needle indicated a source vaporization depth corresponding to the thermocouple location. Results indicated that tracer vaporization of ^{203}HgCl$_2$ in MX4926 occured at a temperature of approximately 300°C.
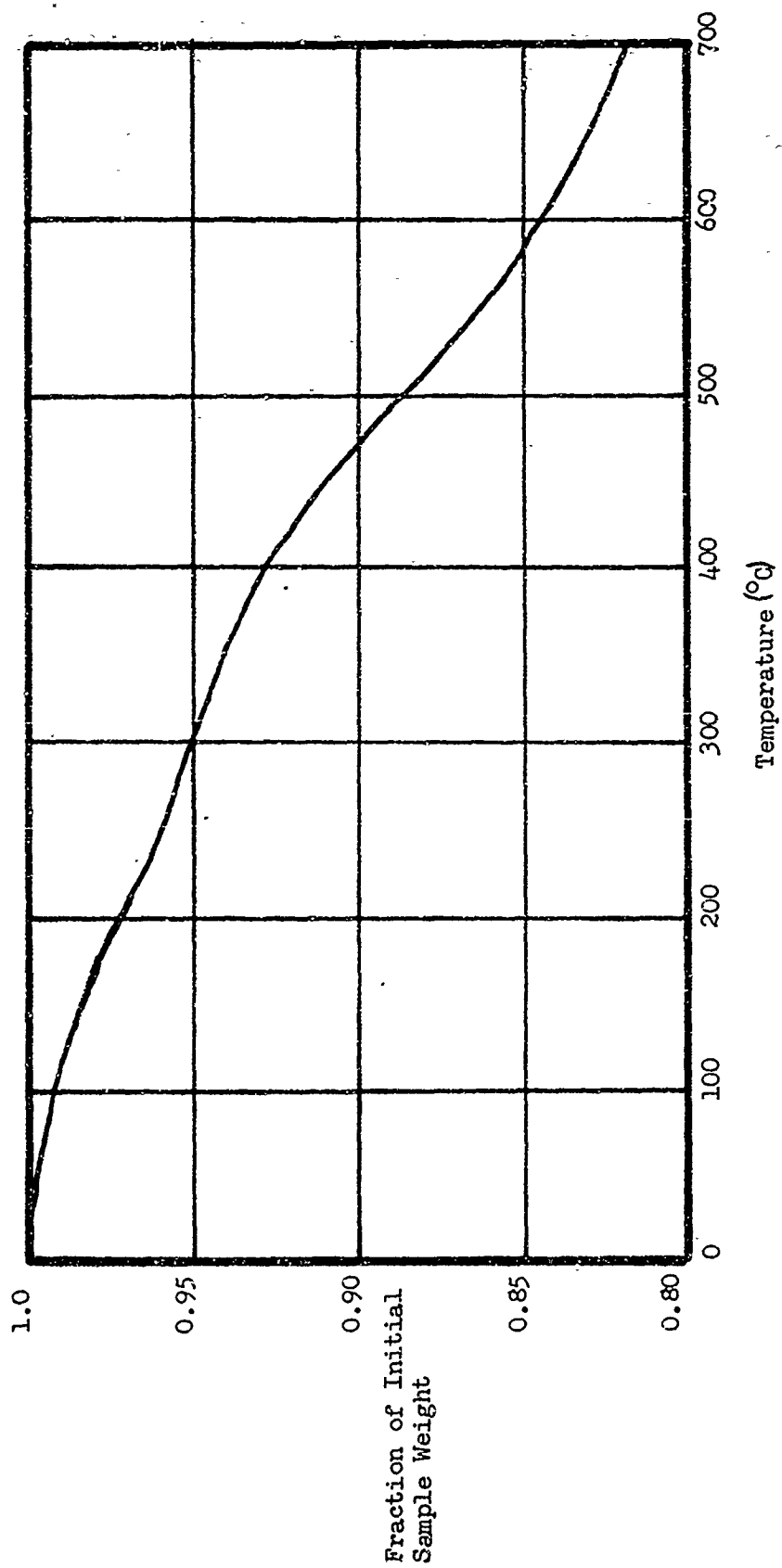
---

*Thermogravimetric analysis

3-13

Figure 10. Data of MX4926 Thermogravimetric Analysis

The observed temperature is consistent with the published value of $302^\circ C$ for the boiling point of mercuric chloride. However, the measured char-depth was only 100 mils whereas the thermocouple registering the $300^\circ C$ temperature was located at a depth of 500 mils. The conditions of this test were duplicated two additional times with the same result.

Because of the test results just described, other mercury compounds with higher boiling temperatures than $HgCl_2$ were evaluated. Mercuric sulfide had been considered and rejected during the Task I studies. Conversion to the form of HgS from the $HgNO_3$ compound received from the supplier was believed to be inconvenient and impractical for this application. However, in the reevaluation, the HgS sublimation temperature of $584^\circ C$ appeared to be reasonably consistent with the temperature necessary for char-front measurements. The advantages of lower cost and relative biological toxicity offered by ^{203}Hg versus $^{113}Sn-^{113}In$ out-weighed the possible chemical conversion problems associated with mercuric sulfide. For these reasons, experimental studies were also conducted with HgS as the ablation radiotracer.

Needles containing ^{203}HgS were flame-tested and their response to the heat flux found to be almost identical to that of the needles containing mercuric chloride. After verifying that the radiochemical tracer was indeed fully-converted mercuric sulfide, additional flame tests with HgS were conducted with the same results.

The program scope did not permit extensive chemical investigations to determine why the HgS tracer was volatilizing at temperatures on the order of $300^\circ C$. Therefore, experimental studies were initiated with the $^{113}Sn-^{113}In$ ablation radiotracer.

3.3.2.2 Tin-Indium Ablation Tests

The decay mode of ^{113}Sn shown in Figure 11, is by electron capture to a metastable state of $^{113}In^{M*}$. The de-exitation of the ^{113}In isomer to its ground state occurs with a half-life of 104 minutes

---

*The symbol ^{113}Sn as used throughout the text actually refers to the metastable state of this isotope (i.e., $^{113}In^{M}$) since the stable ground state is of no interest from a gauging standpoint.

through emission of a 0.392 Mev gamma photon. In the ablation flame tests with ^{113}Sn-^{113}In, radiation measurements are made of the 0.392 Mev isomeric transition gamma of ^{113}In^M.

Figure 11. Decay Scheme of ^{113}Sn
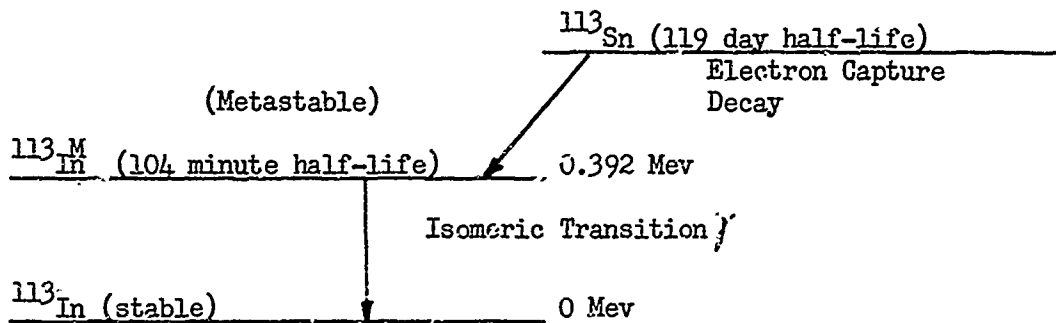
Preparation of the ^{113}Sn-^{113}In radiotracer was simply an evaporation of the SnCl$_2$ solution as received from the supplier. Hence, ^{113}Sn and all ^{113}In activity from the solution were in chloride form. However, since additional radioactive indium is formed continuously through the ^{113}Sn decay process, the ^{113}In atoms formed after needle fabrication might possibly be in many chemical forms. The most probable form, however, is the chloride and experimental results supported this contention.

A freshly purified sample of ^{113}Sn will form ^{113}In^M with the following relationship:

$$N_d^t = \frac{\lambda_p}{\lambda_d - \lambda_p} N_p^o (e^{-\lambda_p t} - e^{-\lambda_d t}) \qquad (2)$$

where:

N_d^t = number of daughter atoms at elapsed time, t

λ_p = decay constant of the parent specie $(0.693/t_{1/2}$ parent)

λ_d = decay constant of the daughter specie $(0.693/t_{1/2}$ daughter)

N_p^o = number of parent atoms at zero time (i.e., purification time)

t = elapsed time units since parent purification

$t_{1/2}$ = half-life; time required to reduce specie population by one-half

Equation (2) includes terms showing both daughter growth and daughter decay. As can be seen from this equation, the term of daughter decay, $e^{-\lambda_d t}$, becomes negligible compared to $e^{-\lambda_p t}$ when t becomes sufficiently large. For the two isotopes of interest, this occurs within a few hours (see Figure 12). In such a case, equation (2) can be expressed by:

$$N_d^t = \frac{\lambda_p}{\lambda_d - \lambda_p} \, N_p^o \, e^{-\lambda_p t} \qquad (3)$$

In this situation, called secular equilibrium, the daughter specie appears to decay at the rate of the parent. If the daughter specie were extracted from the equilibrium mixture, it would follow its own characteristic decay equation of:

$$N_d^t = N_d^o \, e^{-\lambda_d t} \qquad (4)$$

where:

N_d^o = number of daughter atoms at zero time, i.e., extraction time

Figure 12 illustrates the parent-daughter situations described in equations (2), (3), and (4). From the figure, it is evident that equilibrium is attained within about 10 hours after separation, or any other operation that might result in the preferential retention of either isotope. Hence, there is no question that equilibrium decay conditions prevail in the needles at the time of test.

To use $^{113}Sn-^{113}In$ as an ablative gauging tracer one must consider the differences in boiling points of the two compounds and compare the anticipated test duration to the $^{113-M}In$ half-life. With a nominal 60-second test time, deviations from equilibrium would not be apparent during the test regardless of differences in boiling points, because the period is short compared to the half-life. In addition, stannous chloride boils at $623^\circ C$ and indium mono-, di-, and tri-chloride boil throughout a temperature range from 550-600$^\circ C$. Therefore, even without the very favorable ratio of $^{113-M}In$ half-life to test duration, it would be difficult to preferentially volatilize the indium

Figure 12. ^{113}Sn-^{113}In Secular Equilibrium
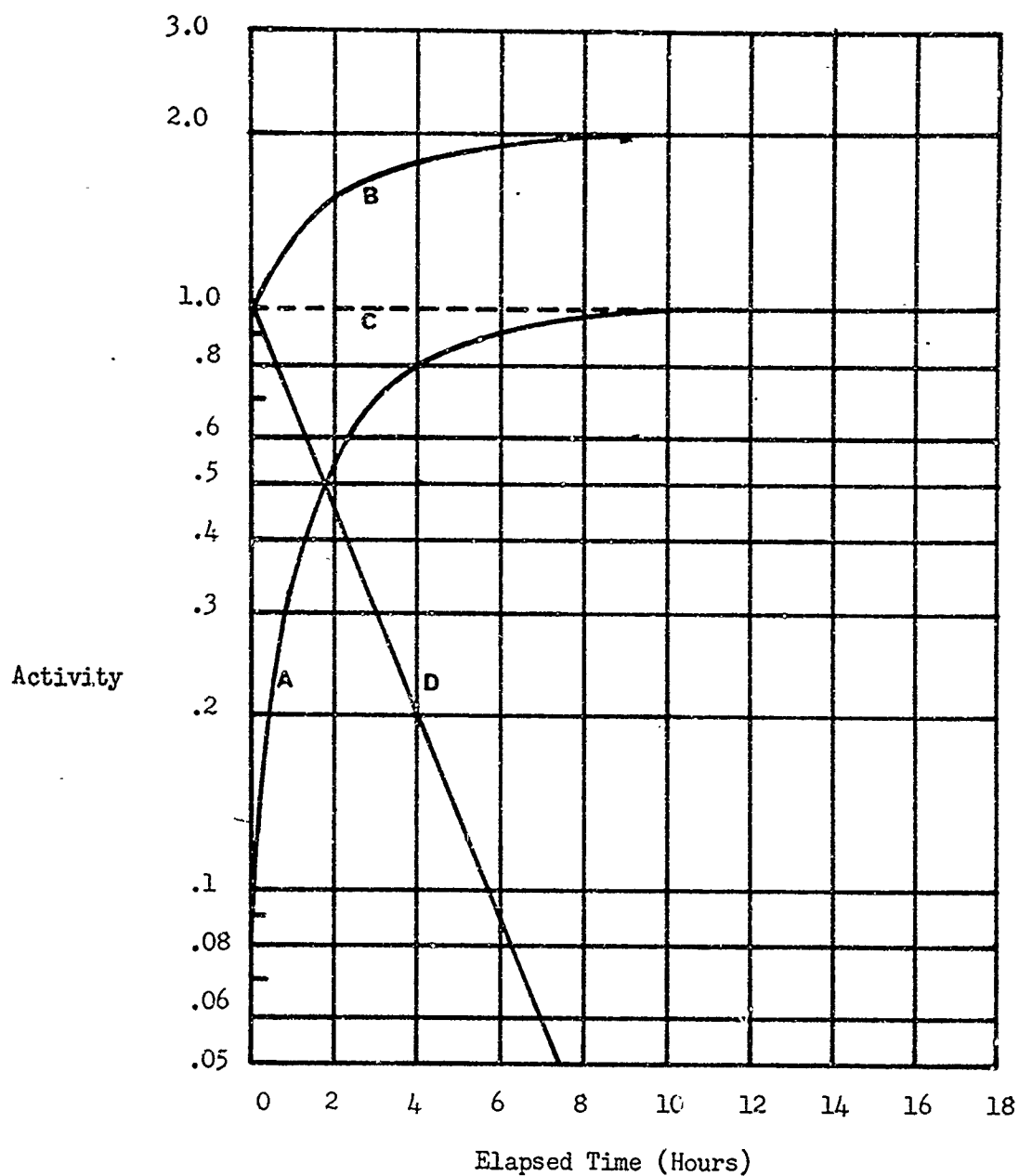
A = ^{113}In growth in pure ^{113}Sn sample

B = Total activity in sample

C = Activity due to ^{113}Sn

D = Decay of daughter extraction

3-18

to any appreciable extent except by limiting the temperature of a large portion of the needle to the range of 550 to 600°C. This is highly improbable during a rocket engine test, because very sharp thermal gradients are produced by the high incident heat flux. However, it was possible to observe daughter isotope growth in the laboratory during prolonged flame-test interrupts. After exposing an ablation test sample to the oxyacetylene flame, a count rate increase was noted during extended post-test cooling periods, confirming that the daughter is indeed present in a chemical form which boils at a temperature below that of the ^{113}Sn parent. However, it should be reiterated that this effect was not detectable during the test itself not did it in any way decrease the accuracy of the dynamic measurements.

Radioactive needle ablation tests with the tin-indium tracer showed good agreement between char-front and tracer ablation. Figure 13 shows data from a typical ablation test; the figure compares physical measurements to radiotracer ablation as determined by ^{113}In count rate. There were two separate physical measurements made at each count rate data point. Based on the ten-point sample, the standard deviation of the ablation gauge errors was 17 mils. This error is defined as the difference between a physically measured ablation depth and that determined by radiotracer measurements. With the 1-inch needle used for this test, the standard deviation is equivalent to a 1.7 percent error.

3.3.3 Concurrent Ablation/Erosion Flame Tests

After measuring and confirming the response of needles containing individual radiotracers, flame tests were conducted with needles which contained both tracers in the manner previously described. Before testing, the physical characteristics of the needles were evaluated. Digital count rate data were obtained during the test for subsequent comparison with the physical measurement data.

Figure 14 illustrates the detected gamma energy distribution of a typical ablation/erosion needle and indicates the location of the energy "windows" used to observe each of the radiotracers. To determine the loss of the 0.392 Mev ablative tracer from the needle, one must account for the count rate contribution due to the down
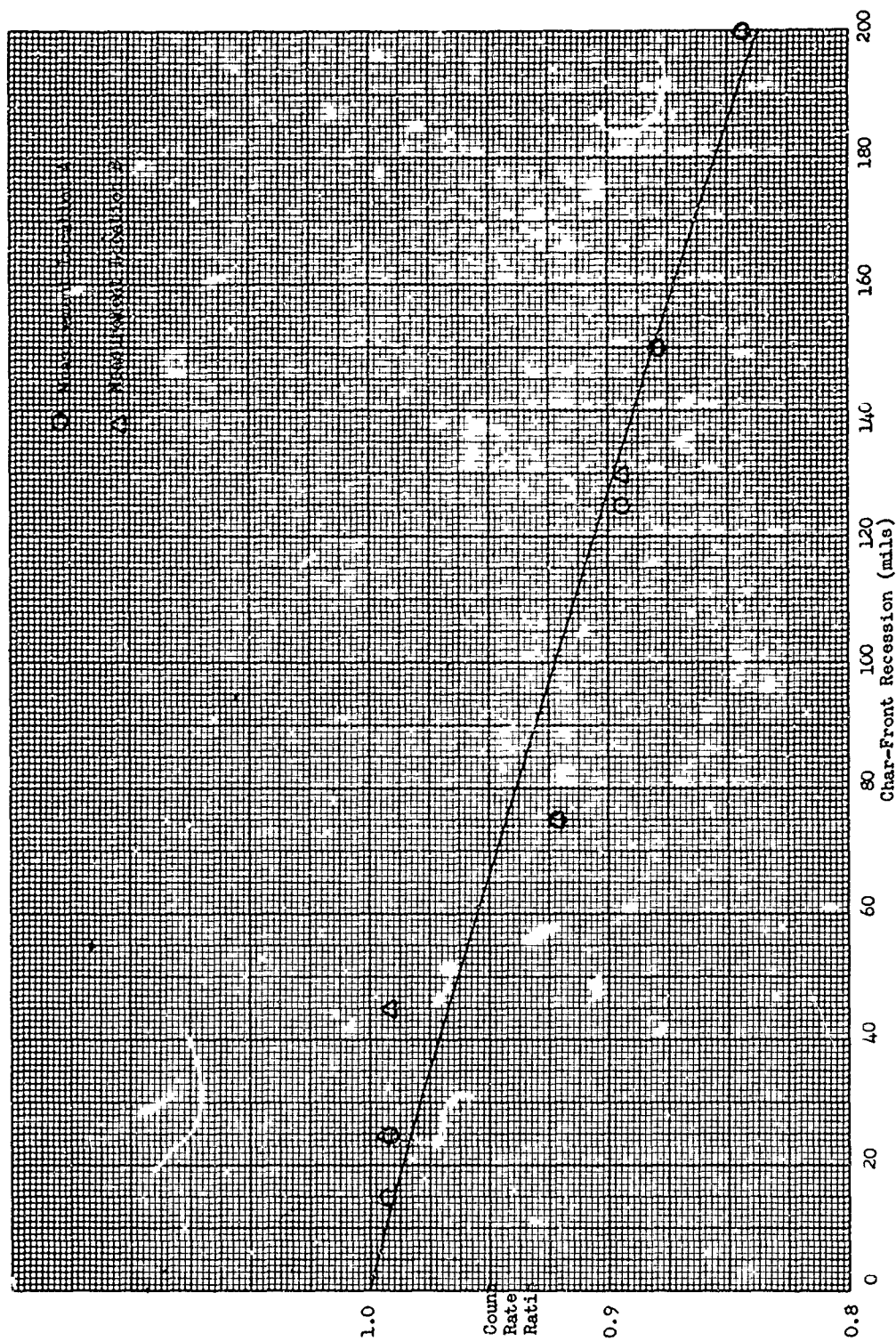
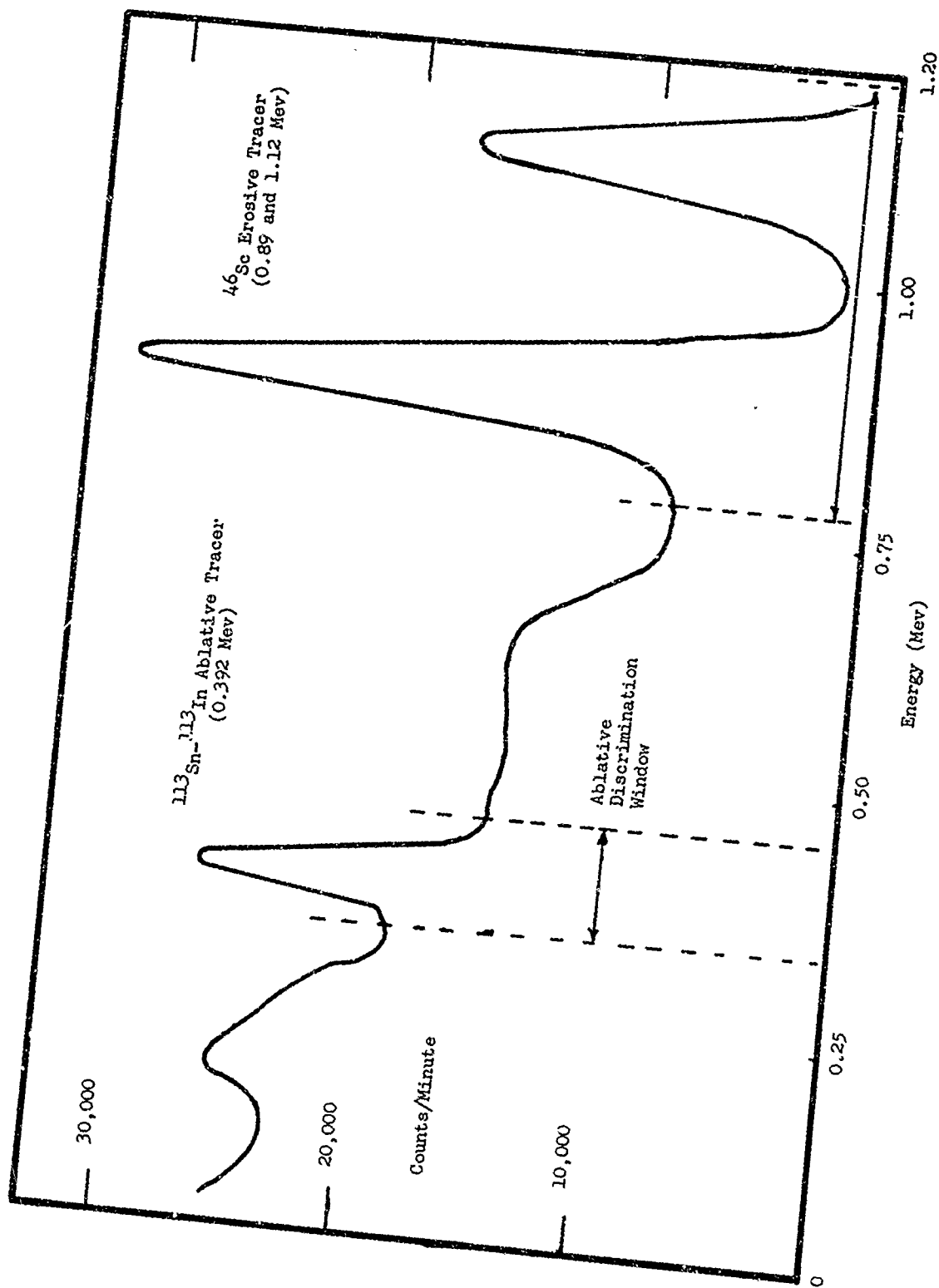Figure 13. Flame-Test Ablation of 1.0 Inch Needle

Figure 14. Gamma Distribution of Ablation/Erosion Needle

3-21

scattering of the higher energy (0.89 and 1.12 Mev) ^{46}Sc erosive tracer gamma rays. To establish this correction factor, the ^{46}Sc gamma intensity was measured as a function of gamma energy. For the physical conditions of a 5K engine test, it was determined that for every 1000 counts recorded within the ^{46}Sc photopeak region, 363 counts would be recorded in the ^{113}Sn-^{113}In discrimination window.

Typical test data from a needle containing the ^{113}Sn-^{113}In ablative tracer and the ^{46}Sc erosive tracer are illustrated in Figure 15 and 16. These figures show the fractional count rate for each isotope as a function of the actual physical measurements from the flame test of a 0.8-inch needle. Theoretical curves are shown by the solid lines in each figure. Experimental data points are corrected for background and, as discussed above, the gamma contribution of the erosive tracer to the ablative tracer count rate. The eight data points gave an average error of 9 mils; maximum disagreement was at the third erosion point which indicated a physical erosion depth 20 mils greater than that indicated by the counting rate. The data indicate that concurrent ablation/erosion measurements should not significantly influence the quality of the gauging technique.
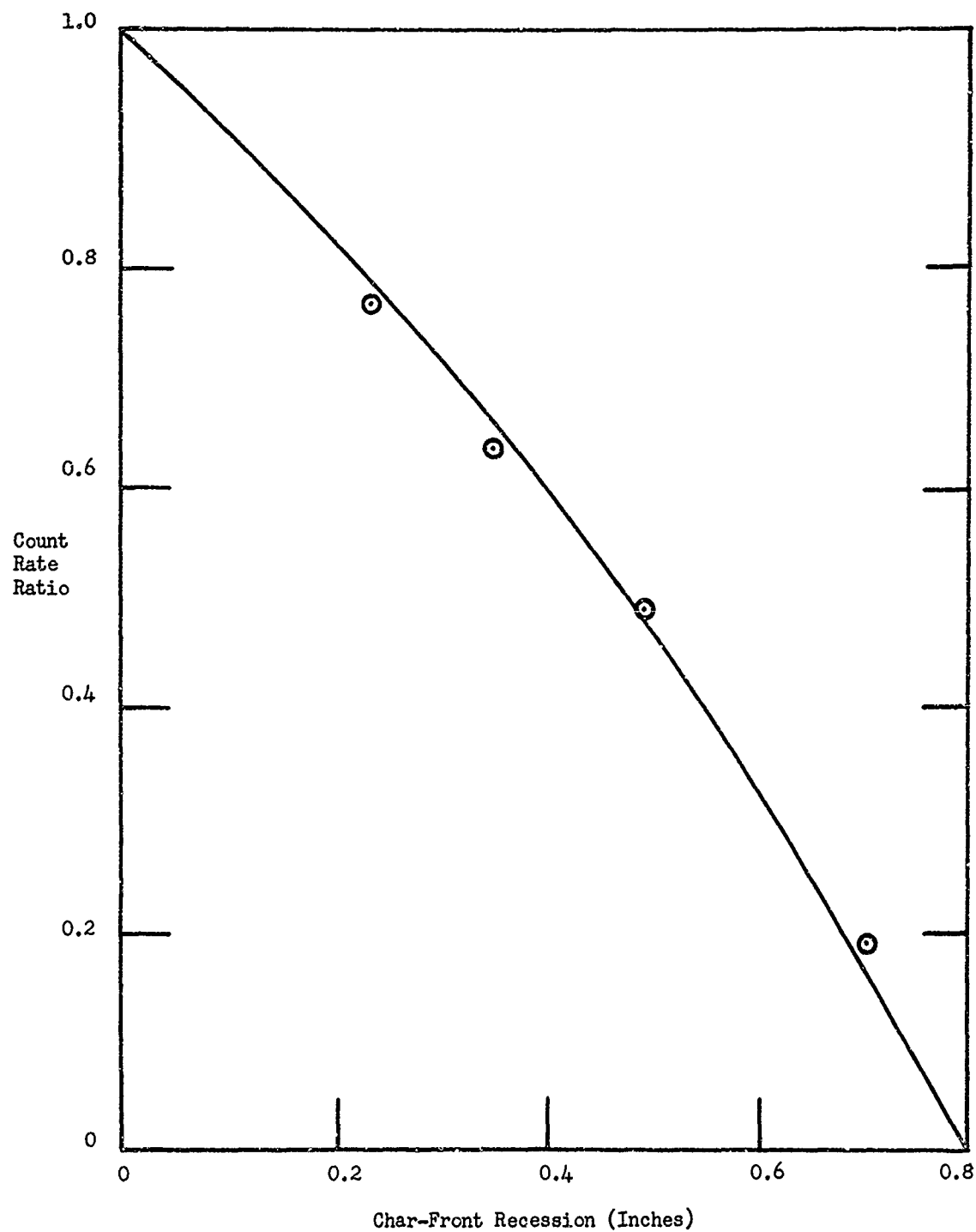
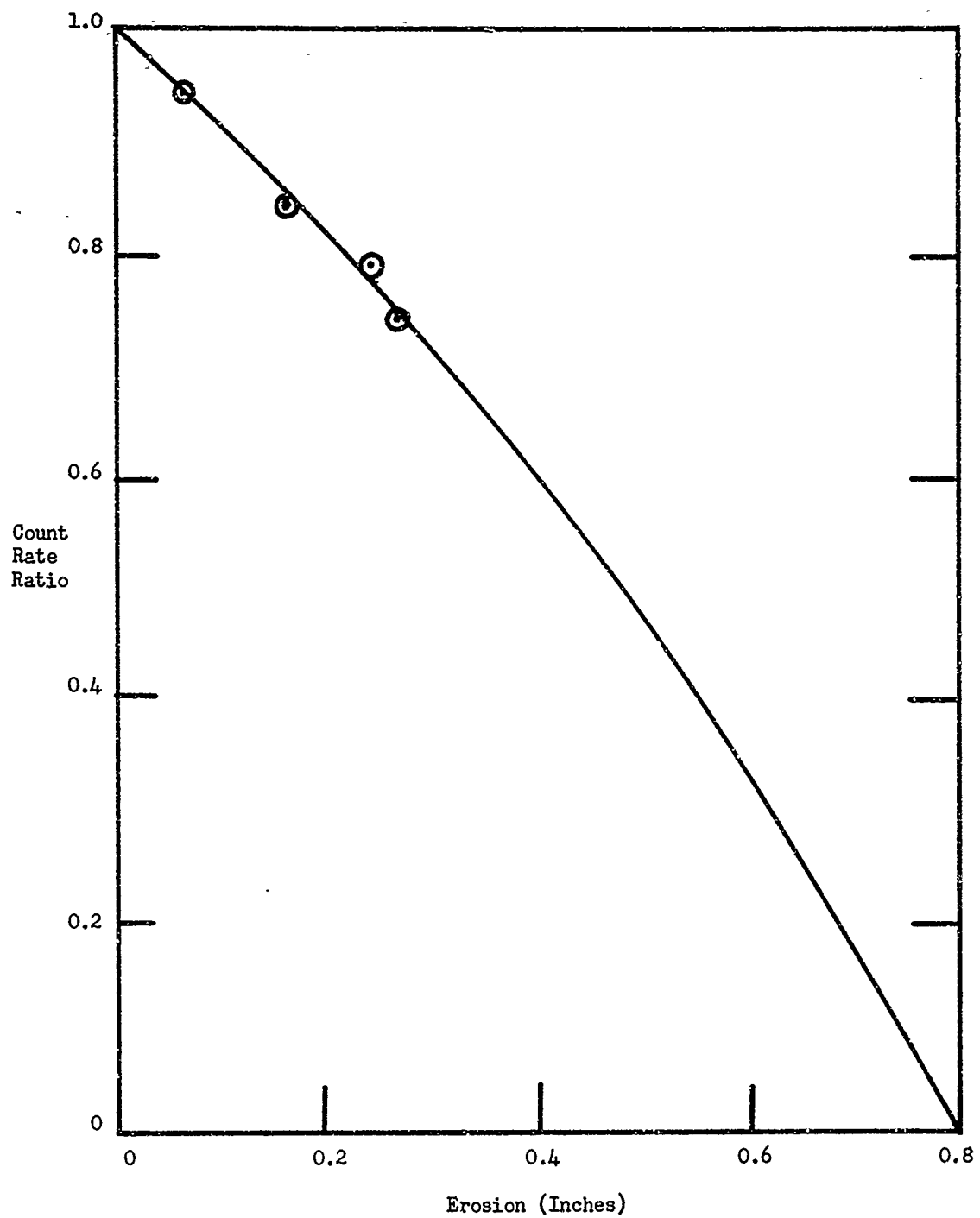Figure 15. Recession Gauging Measurements,
Ablative Tracer

3-23

Figure 16. Recession Gauging Measurements,
Erosive Tracer

3-24

Laboratory testing of the radiotracer ablation/erosion gauging technique has shown that recession sensor needles can be satisfactorily fabricated from MX4926 ablative material constituents and radiotracer additives. In addition, measured radiotracer count rate reductions from flame-test needles can be correlated to the physically-measured ablation and erosion rates with high accuracy. Maximum errors were usually less than 20 mils, with the average errors typically less than 10 mils. The agreement between count rate gauging and physical measurements in the laboratory phase of the program will give added confidence to recession gauging data from the 5K rocket engine tests.

1. R. A. Florentine, et al, "Radioactive Ablation Sensors: I. Radioactive Dispersions", Second Annual AIAA Meeting, San Francisco, California (July 1965)

2. P. J. LeBel, "Feasibility Tests of a Radioisotope-Type Ablation Measuring System", P 28-41, RADIOISOTOPES FOR AEROSPACE Part 2: Systems and Applications (J. Dempsey and P. Poleshuk ed.) Plenum Press, New York (1966)

3. G. Lang, "Development and Fabrication of Char Progression Sensors", Final Report of NASA Contract NAS 9-2610, Emmerson Electric Report No. 1700A (September 1964)

4. W. Brandon Jr., "Heat-Shield Ablation Measurements Using Radioisotope Techniques", NASA TND-3329 (March 1966)

5. W. G. Davis, "Determination of Heat-Shield Char-Front Recession with a Nucleonic Technique", NASA TND-3264 (March 1966)

6. THE USE AND PERFORMANCE OF HITCO ABLATIVE MATERIALS, H. J. Thompson Fiber Glass Company Publication

7. G. W. Sykes, Jr., "Decomposition Characteristics of a Char-Forming Phenolic Polymar Used For Ablative Composites", NASA TND-3810 (February 1967)

INCREMENTAL UNIFORMITY ANALYSES

Successful application of the radiotracer ablation gauging technique requires uniform radiotracer distribution throughout the entire needle length. Tracer uniformity is determined by measuring the radiation intensity of a needle segment through a slit collimator of lead. Source gammas are attenuated by the lead along the needle length except for that increment located in the slit. The needle length is moved in increments past the slit with a depth micrometer.

Since gamma attenuation is a negative exponential function of absorber mass, some photons will pass through significant absorber thicknesses. Therefore, the gamma flux emerging from the slit collimator is not due exclusively to the needle segment located within the slit. Theoretical analyses of this attenuation geometry consider the line-source to be made up of number of "point-source kernels". The total unattenuated gamma flux at the detector is then obtained by integration of the point kernels along the line source. However, this type of analyses yields only the uncollided flux and does not account for those gammas which have been scattered one or more times before being detected. Hence, experimental measurements of "point-source kernels" were employed in the uniformity analyses. With these measurement data, it was possible to duplicate the data which would result from measurements of a uniform needle.

To determine the total count rate contribution from needle segments which are not within the slit, the gamma intensity of a 100-mil needle length (i.e., 100-mil kernel) was measured as it traversed throughout the collimation jig having a 100-mil slit. Figure I-1 was obtained by such measurements. With data of incremental count rate contributions and knowledge of needle length and location in the jig, one can calculate what fraction of the total gamma intensity from a uniform needle emmanates from that needle within the slit. Figure I-2 illustrates the count rate measurements from a 1 inch needle as it traversed the slit collimator. Figure I-3 shows data variations about the mean corrected count rate after the attenuated gamma contribution was analytically removed from gross count rate data.
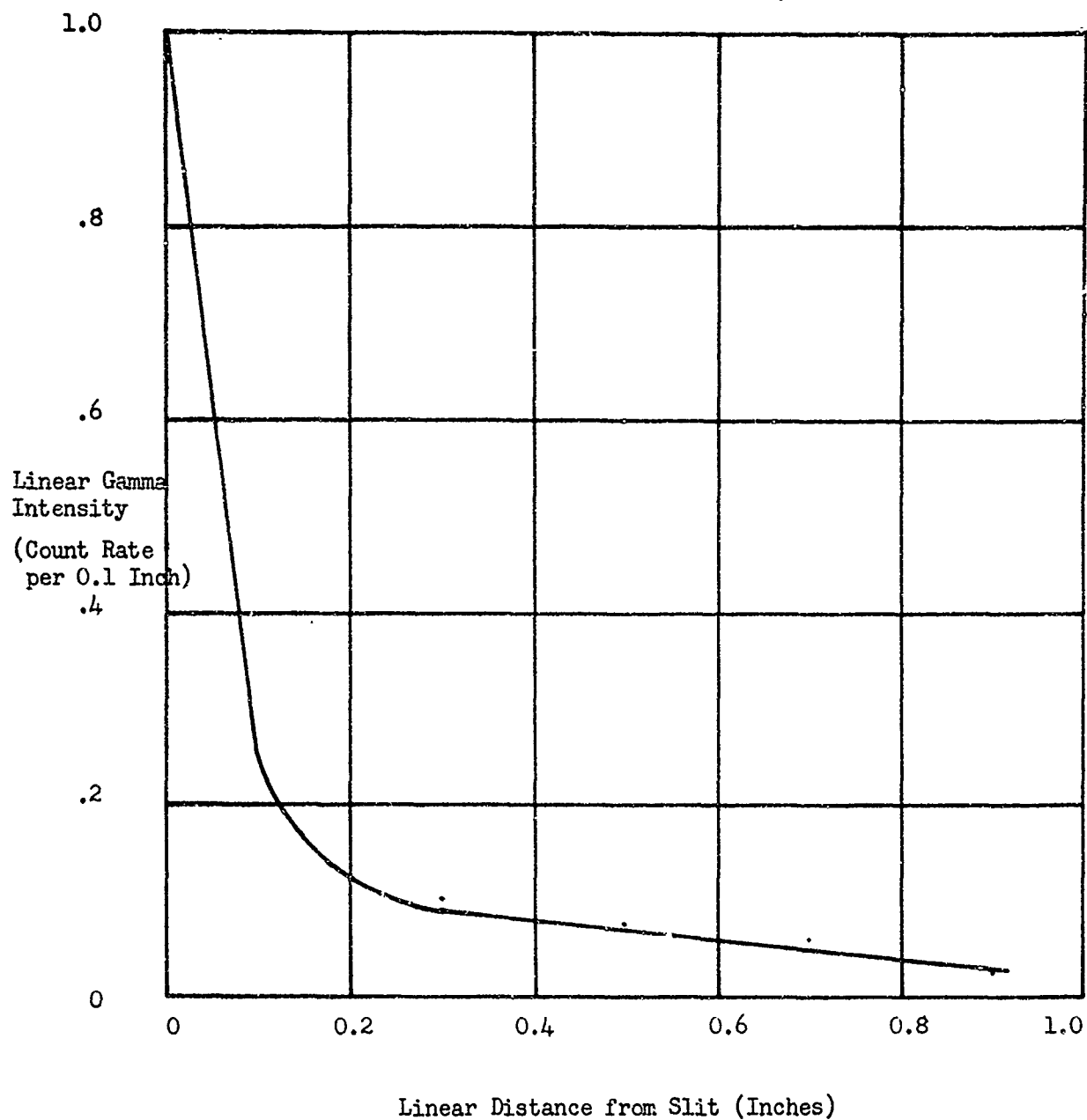
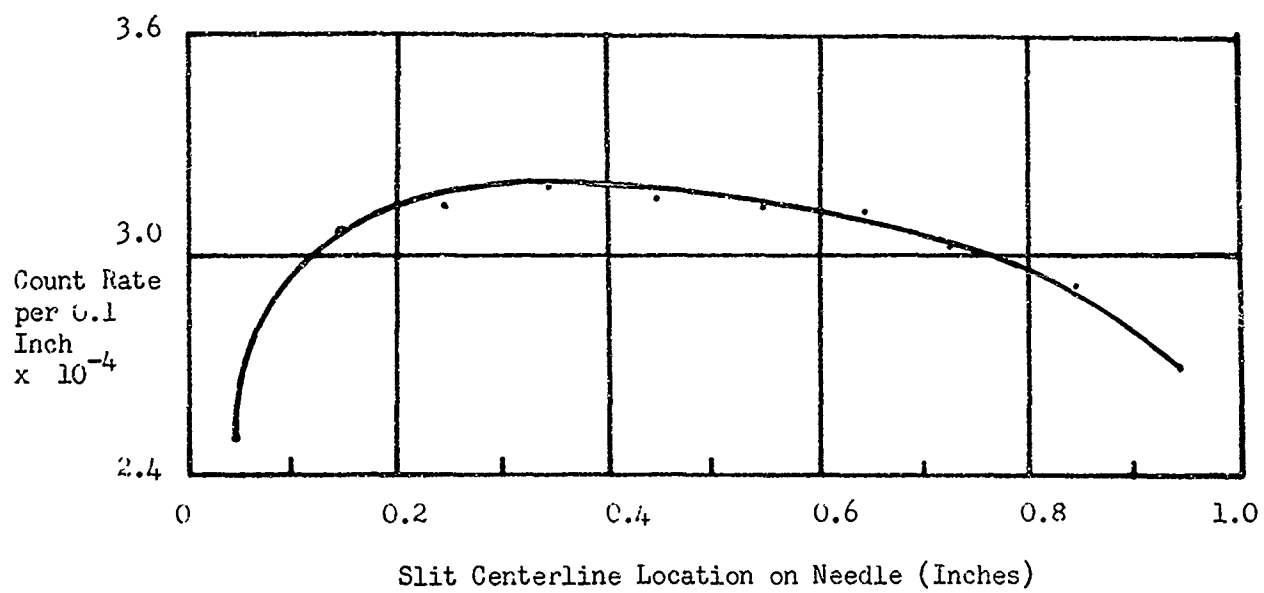Figure I-1. Kernel Count Rates Through
Slit Collimator
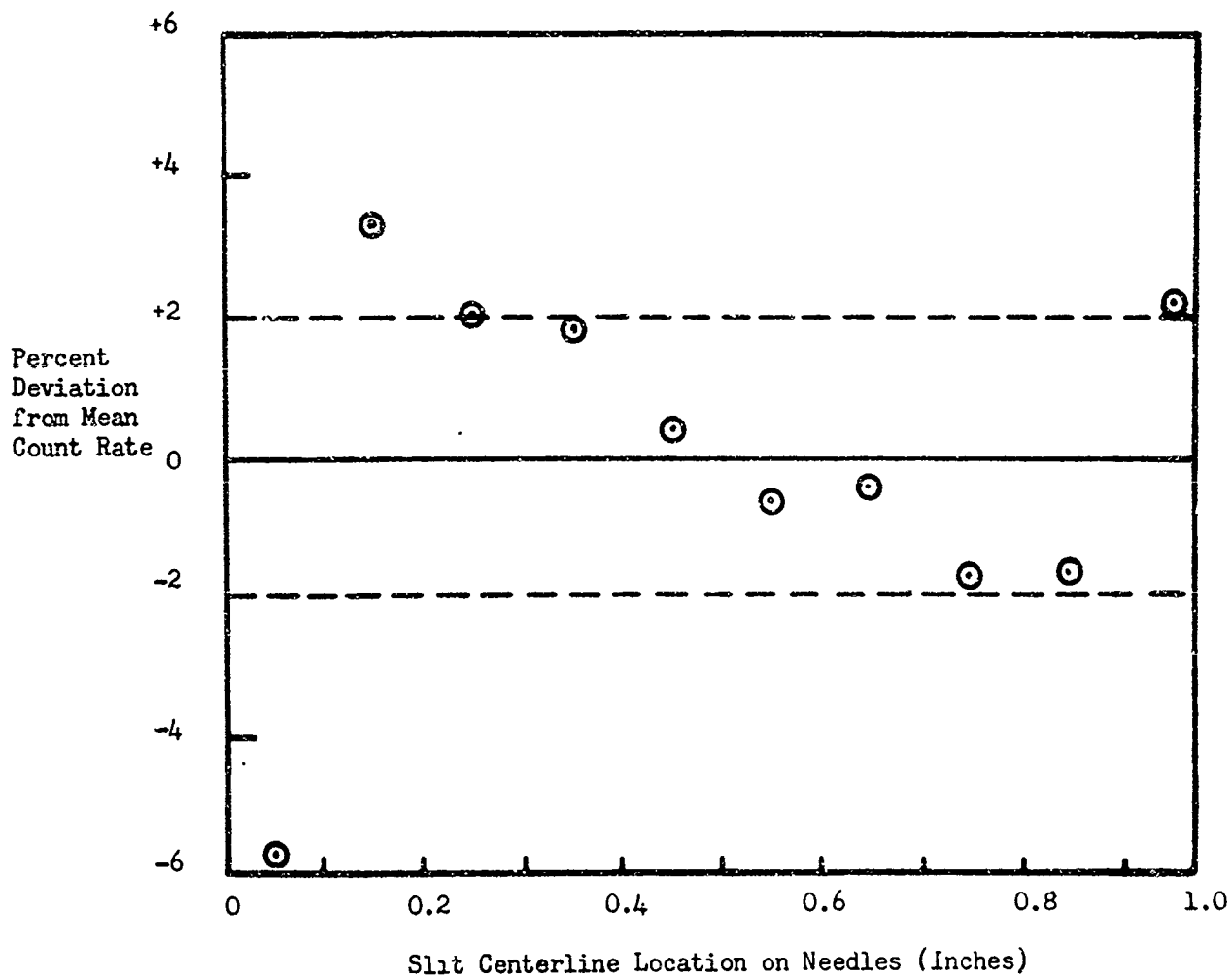
I-2

Figure I-2. Count Rate Measurements of Needle Kernels

Figure I-3. Needle Incremental Uniformity

I-4